Aristotle University of Thessaloniki
Faculty of Sciences
Department of Physics

Bachelor Thesis

Author:
Kasapakis Nikolaos[1]

Supervisor:
Prof. Theodoros Samaras[2]

Insert Title Here

July 18, 2024

Aristotle University
of Thessaloniki
SCHOOL OF PHYSICS

[1] nkasapak@auth.gr, *https://github.com/kasapakis-nk*
[2] theosama@auth.gr

mythesis

Nikos Kasapakis

May 2024

This page intentionally left blank.

Abstract

Insert title here

Kasapakis Nikolaos

Insert my abstract text here.

This page intentionally left blank.

Περίληψη

Βάλε τίτλο εδώ

Κασαπάκης Νικόλαος

Βάλε κείμενο εδώ.

This page intentionally left blank.

Acknowledgements

I want to thank Proffessor Samaras, Dimitris Stoupis (include all titles), Ioanna K.

This page intentionally left blank.

Contents

This page intentionally left blank.

List of Figures

This page intentionally left blank.

List of Tables

This page intentionally left blank.

Listings

Chapter 1

Theoretical Background

1.1 Introduction

The significance of the sense of vision for humans, in our contemporary everyday lives as well as in our evolution as a species, cannot be understated. While there is no clear consensus that vision is our most important sense, since that is dependent on one's cultural, societal and technological influences, there exists a large body of data drawn from cross-sectional observational research and surveys, as well as expert opinion of practitioners and researchers that leans towards the fact that vision is considered the most valued sense to the general public.

Since prehistoric times, it is our vision that has aided us in our survival, by means of allowing us to advantageously select healthy mates, forage ripe fruit against a green foliage and detect predators through their natural camouflage, just to name a few benefits. Even in today's world, the majority of the information we process hails from our eyesight, whether it originates from the envirorment or from a computer screen.

However controversial the topic of the superiority of vision over our other senses might be, what is truly undebatable is that our evolution and eventual dominance as a species has been a consequence of the capabilities of our brain. It is the current form of the human brain after all, displaying an astonishingly intricate way in which it processes visual stimuli, that was preferentially chosen through natural selection to translate visual information to fit the species' best interests. Thus, it could be argued that to achieve a holistic understanding of the sense of vision, we need to delve into the patterns of activation induced in the brain by visual stimulation.

1.2 Visual Information Flow In The Brain

Light entering the eye creates a cascade of neuronal events throughout the optic pathway, which describes the anatomical pathway by which electrical signals generated by the retina are sent to the brain.

1.2.1 The Optic Pathway

The optic pathway begins in the retina, which is a complex structure made up of ten different layers. Noteably, the photoreceptor layers consist of the rods and cones, which generate action potentials with the help of rhodopsin through photosensitive cycles. The ganglion cell layer and nervefiber layer serve as the foundation of the optic nerve; the former contains the cell bodies, and the latter contains the axons as they stream across the retina. The nerve is surrounded by the dura, which is a continuation of that of the brain, allowing free movement of Cerebrospinal Fluid (CSF) between the eye and the intraclanial vault. The axons exit the orbital part of the optic nerve through the orbital foramen, simultaneously with the ophthalmic artery and sympathetic fibers.

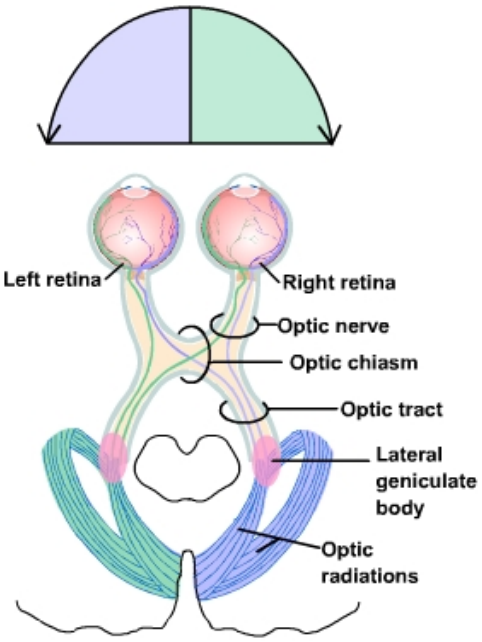

Figure 1.1: Illustation of the Visual Pathway and its components, including the course of information flow from the right (green) and left (blue) hemifields of the two eyes' visual fields. **no DOI cite Neuroscience Online Tsuchitani and Dragoi Ph.D.**

They then enter the optic canal, a bone-encased tunnel intended to protect the nerve, exit into the middle cranial fossa to form the intracranial part of the optic nerve, which continues till the two optic nerves join together to form the optic chiasm directly behind and above the pituitary stalk. Beyond the chiasm, the pathway continues as two distinct tracts, each carrying the temporal fibers from the other eye. The optic tract then passes posteriorly where most of the axons synapse in the layers of the Lateral Geniculate Body (LGB) of the midbrain, which is a posterolateral extension of the thalamus.

The majority of the fibers pass posteriorly to become the genico-calcarine tracts, which have both parietal and temporal loops and terminate into the cuneus gyrus and lingual gyrus of the primary visual cortex, respectively (see Figure 1.1). Perception of sight ultimately derives from processing within this and adjacent areas of the brain [1].

1.2.2 Information Processing In The Visual Cortex

The modules that compose the visual pathway from the retina to higher visual centers follow two diverging streams in the cortex: one pathway extends dorsally to terminate within the parietal lobe, including the motion detection area, Middle Temporal visual area (MT), and the visual areas of the posterior parietal cortex; the other pathway extends ventrally to terminate in the temporal lobe, including V4 and Inferior Temporal cortex (IT). It is suggested [2] that these two pathways serve different functions: the dorsal pathway is concerned with *where* an object is in visual space (motion, distance); the ventral pathway is concerned with *what* an object is (form, color, texture, all of which are involved in object recognition) (see Figure 1.2).

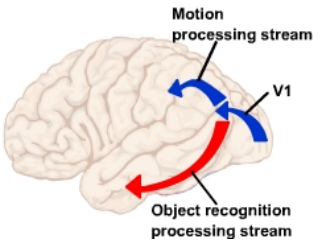

Figure 1.2: Distinction in the flow of visual information from the V1 to other cortical areas. The ventral stream transfers information to the inferior cortical areas, whereas the dorsal stream tranfers it to the more superior cortex.

The V1 area of the brain is involved in the initial cortical processing of all visual information necessary for visual perception. The color, shape and movement information from the thalamus are sent to different neurons within V1 for further processing and then sent onto different areas of the extrastriate visual cortex.

Within V1, information processed by blob cells is used in color perception, color discrimination and the learning and memory of the color of objects. The blob cells are the "color" processing cells of the V1. On the other hand, V1 interblob cells belong in one of two categories: The first are location specific cells, which respond best when the stimulus is in a specific location of the receptive field. The information processed by these cells is used in object perception, discrimination, learning and memory, or in spatial orientation. These cells are the "shape, form and location" cells of the V1; The second kind of interblob cells is the movement sensitive ones, which respond best to moving stimuli and are utilized to detect object movement, direction and velocity and to guide eye movements. These are the "motion detecting" cells of V1.

The V1 sends input to the extrastriate visual cortex, which includes all of the occipital lobe areas surrounding the V1. The extrastriate cortex in non-human primates has been subdivided into as many as three functional areas V2, V3 and V4. The information corresponding to each of the afformentioned categories of neurons in the V1 is sent to different areas of the extrastriate

visual cortex.

Specifically, the neurons in the inferior temporal visual association cortex, i.e., the ventrally located neurons accessed by the ventral stream, are responsible for processing information necessary for our abilities to recognize objects and colors, read text and learn and remember visual objects. It can thus be concluded that, in the context of this thesis, which investigates task-evoked visual stimulation, this area of the brain will be the region of interest. More deliberately, four regions of extrastriate cortex are of utmost importance for the purposes of this current dissertation: the Fusiform Face Area (FFA), the Parahippocampal Place Area (PPA), the Lateral Occipital Cortex (LOC) and the Extrastriate Body Area (EBA).

1.2.3 Category-Specific Information Processing Areas In The Extrastriate Visual Cortex

In the early 1990s, Positron Emission Tomography (PET) demonstrated activation of the ventral visual pathway, especially the Fusiform Gyrus (FG), in a variety of face perception tasks [3], [4]. fMRI studies of the specificity of these cortical regions for faces began with demonstrations of fusiform regions that responded more strongly to faces than to letter strings and textures [5], flowers [6] and other mixed stimuli [7]. Although face-specific fMRI activations could also be seen in many subjects in the region of the Superior Temporal Sulcus (fSTS) and in the occipital lobe in a region named the Occipital Face Area (OFA), the most consistent and robust face-selective activation was located on the lateral side of the mid-fusiform gyrus, within the IT, in a region consequently named the FFA. With the methods currently used, this region can be functionally identified in almost every normal subject in a short "localizer" fMRI scan contrasting the response to faces versus objects [8].

Another well studied category-selective region of cortex is the PPA, responding strongly to a wide variety of stimuli depicting places and/or scenes (e.g. outdoor and indoor scenes and houses) compared to various control stimuli such as faces or scrambled scenes [9]. Additionally, it has been found that PPA activity is not affected by the subject's familiarity with the place depicted, does not increase when subjects experience a sense of motion through the scene, and is greater when viewing novel versus repeated images [10]. Using sets of scenes that had viewpoint changes, it was demonstrated that the PPA treated scenes with viewpoint changes as different [11], suggesting that this area represents scenes as individual snapshots of each view rather than as a broader scene that integrates multiple similar snapshots. However, when subjects saw different snapshot views from panoramic scenes, which represented clearly different views but appeared to come from the same scene, fMRI showed no attenuation for panoramic repeats in the PPA, suggesting viewpoint-specificity [12].

The LOC is located on the lateral bank of the FG, extending both ventrally and dorsally, consisting of the Middle Occipital Gyrus (MOG) and the Inferior Occipital Gyrus (IOG) as well as the Lateral Occipital Sulcus (LOS) between them. This region has been shown to respond more strongly when subjects passively view photographs of common everyday objects than when they view visual textures without obvious shape interpretations [13]. Importantly, the magnitude of the response was no different for familiar objects and unfamiliar ones with clear three-dimensional shape interpretations (e.g. Henry Moore sculptures). A similiar result was found using line drawings [14]: stronger responses to three dimensional objects depicted in line drawings, whether familiar or novel, compared to scrambled line drawings. Several more studies provide evidence that the entire LOC region responds more strongly to intact objects with clear shape interpretations, than to control stimuli that do not depict clear shapes [15]–[17].

Since the turn of the twentieth century, neuroimaging studies have identified two brain regions of the extrastriate visual cortex that are highly sensitive to the perception of human bodies and body parts in comparison to other classes of stimuli. These regions are the EBA, which is a body-selective focal region located partly at both the posterior inferior temporal sulcus and the middle temporal gyrus [18] and the Fusiform Body Area (FBA) found ventrally in the fusiform gyrus [19]. Evidence derived from fMRI studies has shown that both areas become significantly activated in response to body and body parts stimuli visually presented in different formats such as photos, line drawings, stick figures and silhouettes compared to control stimuli like faces, tools and scenes [20]–[22]. Additionally, research seems to suggest that the EBA also

participates in more complex functions like body discrimination of self versus others. [23]. It has been suggested that EBA and FBA can be functionally dissociated, with a more selective activation for local body parts in EBA relative to more holistic images of the human body in FBA [24].

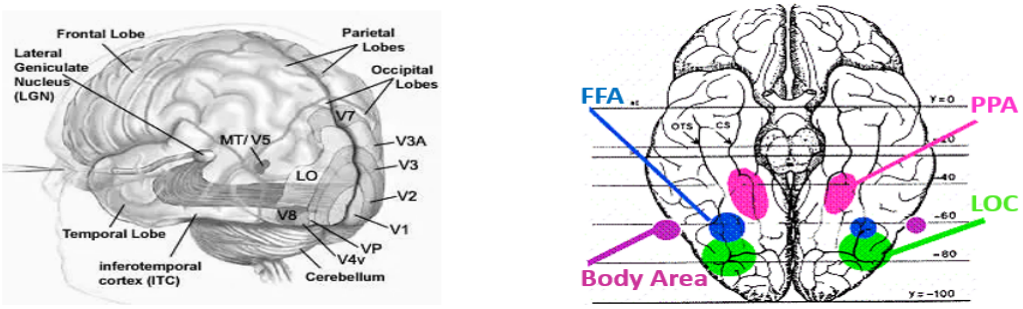

(a) Graphic of the visual areas of the brain thought to be geographically within the occipital lobe [25].

(b) Brain diagram including some category-specific information processing areas of the brain [26].

Figure 1.3: Illustration of ROIs in the human brain.

While it has been clearly established that certain areas of the extrastriate visual cortex process category-specific information (see Figure 1.3), another critical inquiry, particularly in the context of fMRI Multi-Variate Pattern Analysis (MVPA) of contrasts among different classes of stimuli, is whether each region is exclusively selective for target-speific stimuli or if there is overlap between regions, especially considering the close proximity among them. One such case is the FFA and FBA, which have been found in many subjects to be adjacent or overlap with one another. However, in ROIs that ommit overlapping voxels it has been demonstrated [27] that, FFA showed no response above control objects for body stimuli and FBA showed no response above control objects for face stimuli, confirming strong selectivities in distict but adjacent regions in the FG. Similar conclusions of high selectivity have been reached [28] in regards to the FFA and the PPA, where results revealed distinct response properties between the two regions for faces and houses respectively, implying a combination of spatially discrete domain-specific and relatively distributed domain-general organization mapping in the human ventral temporal cortex.

Many brain imaging tools are available to cognitive neuroscientists, including PET, Near Infrared Spectroscopy (NIRS), MEG, EEG and fMRI [29]. Some of those have had their time in the spotlight in the previous decades but have now been oveshadowed by the more advanced, non-invasive neuroimaging techniques such as EEG and fMRI, which allow researchers to direcctly observe brain activities while subjects perform various perceptual, motor or cognitive tasks. It is therefore imperative that we aqcuire at least a basic understanding of the procedures and metrics through which these techniques work if we are to be able to interpret their results and further analyze them. For the purposes of this paper, we focus on the inner workings of fMRI, which is the instrument used to extract the data used in our MVPA.

1.3 Mechanisms of Functional Magnetic Resonance Imaging

1.3.1 Fundamentals of NMR Signal Generation

The outline of the process by which fMRI signal is generated begins with the scanner creating a powerful magnetic field $\vec{\boldsymbol{B_0}}$. All magnetic moments of nuclei with nonzero spin, including protons which are found overwhelmingly in the form of hydrogen nuclei in the human brain, tend to weakly align with $\vec{B}_0$, creating a net macroscopic magnetization $\vec{\boldsymbol{M_0}}$. A coil within the machine, then transmits a radio frequency (RF) transverse magnetic field at the resonant frequency $\omega_0 = \gamma \cdot B_0$, where $\boldsymbol{\gamma}$ is the gyromagnetic ratio, tipping the magnetic moment from alignment and causing it to precess around the $\vec{B}_0$ axis at angular frequency $\boldsymbol{\omega_0}$. For protons, $\gamma = 2.675 \times 10^8\,\mathrm{rad\,T^{-1}}$ and at a typical magnetic field strength of 3 T, the precession frequency

$\nu_0 = \omega_0/2\pi$ is approximately 128 MHz. Following this interaction, the net magnetization vector can be described as two components: the remaining longitudinal magnetization along the $\vec{B_0}$ axis; and the rotating transverse magnetization perpendicular to $\vec{B_0}$. The rotating component generates an oscillating magnetic field that induces a current in a nearby coil, thereby producing the basic measured NMR signal. Over time, the transverse magnetization decays exponentially with a characteristic time constant $\boldsymbol{T_2}$, and the longitudinal magnetization recovers exponentially towards its equilibrium value M_0 with a time constant $\boldsymbol{T_1}$ [30], [31].

1.3.2 Relaxation Time Constants

T1 relaxation is the process by which the z component of the net magnetization M returns to its initial maximum value M_0 parallel to B_0. It can be modeled as a simple exponential with $T1$ as a first-order time constant, defining it as the time required for M_z to reach $(1 - \frac{1}{e})$ or about 63% of its maximum value (see Figure 1.4 [32]). A typical value for $T1$, inside a 3 T magnetic field, in gray matter of the human brain is about 1.0 s. As M_z grows toward M_0 the energy of the spin system decreases, considering that more spins statistically favor the spin-up parallel orientation, which is the lower of the two potential energy states. Consequently, as T1 relaxation occurs, energy dissipates from the system in the form of heat, hence the synonym for T1 relaxation, "thermal relaxation". This heat is then transferred to nearby nuclei via collisions, rotations, or electromagnetic interactions, and becomes unrecoverable. At its core, T1 relaxation represents an energy exchange process between spins and their external environment.

Blood inflow and Cerebral Blood Flow (CBF) can act to decrease the T1 values of blood and extravascular tissue components, resulting in a modified, measured T1 constant, termed T1*. Flowing blood moves spins from outside the imaging plane into the slice pixels. When spins in the imagning plane are saturated, signal from the unsaturated inflowing blood is enhanced relative to the surrounding stationary spins. The magnitude of this inflow contribution in vessels depends on the Magnetic Resonance Imaging (MRI) parameters, TR and flip angle θ. When the TR is sufficiently long to allow arterial blood spins from outside the imaging slice to flow into capillaries and exchange with extravascular tissue water, spatially specific perfusion contrast appears. In the extravascular tissue pool, $\frac{1}{T_1^*} = \frac{1}{T_1} + \frac{f}{\lambda}$ where f is the CBF and λ is the blood-to-tissue partition coefficient [33].

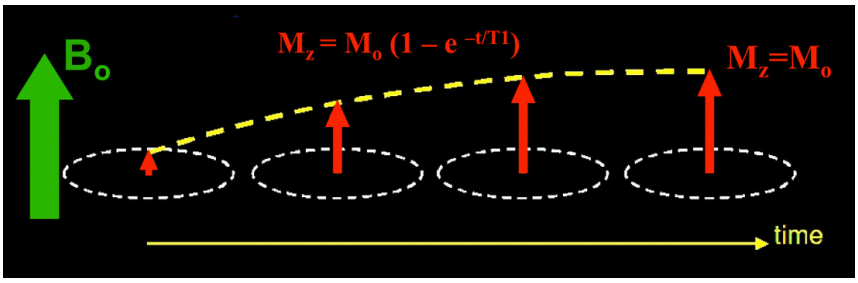

Figure 1.4: Illustration of T1 relaxation.

T2 is the time constant for decay or dephasing of transverse magnetization M_{xy} and may occur with or without energy transfer. T2 relaxation is considered to follow first order kinetics, resulting in a simple exponential decay (identical to radioactive decay), resulting in T2 being the time required for the net transverse magnetization to fall to $\frac{1}{e}$ or approximately 37% of its initial value [34]. Following a 90° RF pulse, the initial Boltzman distribution of spins in the z direction, constituting M_z, is preserved and transformed by the rotation into what is termed "phase coherence" in the xy plane, in the form of an assymetrical clustering of spins which gives rise to a net trasverse magnetization M_{xy}. After the pulse is over, the many transverse spin components will precess within the plane at the Larmor frequency. The presence of a non-zero M_{xy} at any time, is evidence of persistent assymetry of transverse components of angular momentum. Any process that disrupts either the number or the relative positions of said components will result in T2 relaxation. These fall into one of two general categories.

The first kind of T2 relaxation is when it accompanies T1 relaxation. If energy radiated during the latter, were to affect one of the spins contributing to M_{xy}, both its angular momentum components would be randomly changed and it would immediately lose phase relations with other spins, thus it would stop contributing to M_{xy} alltogether. As a result, M_{xy} would be diminished, meaning T2 relaxation would have occured. We can conclude that any process causing T1 relaxation also results in T2 relaxation, while the opposite is not true. This is sometimes called the T1 contribution to T2 and explains why T1 needs to be monitored as well, even though it is the sweep of the transverse magnetization alone that induces a current in the receiver coils, ultimately producing the NMR signal.

On the contrary, stand-alone T2 relaxation is referred to as the secular contribution to T2. One of the most common ways for this to occur is when a spin is situated in a molecular environment where it experiences a local static magnetic field disturbance B_{loc} in addition to B_0. The component $B_{\text{loc}-z}$ of the secondary magnetic field, parallel to the main field, is added to the total magnetic field experienced by the spin, causing it to precess at a frequency $\omega_0' = \gamma \cdot (B_0 + B_{\text{loc}-z})$. Meanwhile, the unaffected spins continue to precess at the original Larmor frequency. Over time, a phase difference of $\phi = \gamma \cdot B_{\text{loc}-z} \cdot t$ develops between the disturbed spin and the rest, leading to loss of phase coherence, T2 relaxation, and reduction in M_{xy}. Secular T2 relaxation can also occur due to a special dipolar interaction, where a pair of spins simultaneously exchange their longitudinal angular momentum components, resulting in no net T1 effect but loss of T2 coherence. In gray matter in the human brain, at a field strength of 3 T, measured T2 is around 0.1 s.

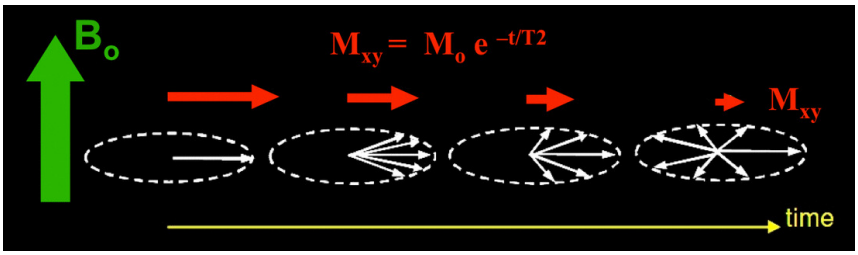

Figure 1.5: Illustration of T2 relaxation.

It needs to be noted that in any real NMR experiment, the transverse magnetization decays much faster than would be predicted by natural atomic and molecular mechanisms; this faster rate is denoted **T2***. It can be considered as "observed" or "effective" T2, whereas the latter can be thought of as the natural T2 of the tissue being imaged. T2* is always less than or equal to T2 (see Figure 1.6). T2* results principally from inhomogeneities in the main magnetic field, which may arise from intrinsic defects in the magnet itself or susceptibility-induced field distortions caused by tissue or other materials within the field. Certain MR sequences using gradient echoes and relatively long Time of Echo values are called T2-weighted (T2w) [35].

Pixel sizes in typical fMRI studies are a few millimeters; each pixel may therefore include blood, extravascular tissue, and CSF. Since arterial blood and venous blood have different T2 values, these should be considered separately, with the assumption that capillary content is partly arterial blood and partly venous blood. Thus, NMR signal intensity from a pixel is the sum of signals originating from multiple compartments with different spin density and relaxation parameters. The fMRI intensity S can be described as seen in Equation 1.1 [36].

$$S = \sum_i \rho_i \times V_i \times M_{\text{ss},i} \times e^{-\text{TE}/T^*_{2,i}} \tag{1.1}$$

$$M_{\text{ss},i} = \frac{\left(1 - e^{-\text{TR}/T_1^*}\right) \sin\theta}{1 - \cos\theta \times e^{-\text{TR}/T_1^*}} \tag{1.2}$$

Subscripts i indicate each compartment; ρ is the water proton spin density, directly related to water content in the tissue; V is the volume fraction, which is approximately 1% for arterial blood [37] and 2.5-3% for venous blood [38], [39]; M_{ss} is the steady-state magnetization given by Equation 1.2; TR is the repetition time; T_1^* is the apparent longitudinal relaxation time in the

presence of inflow; and θ is the flip angle. It should now be evident that fMRI signal changes depend not only on imaging parameters but also on biophysical responses that significantly affect these variables.

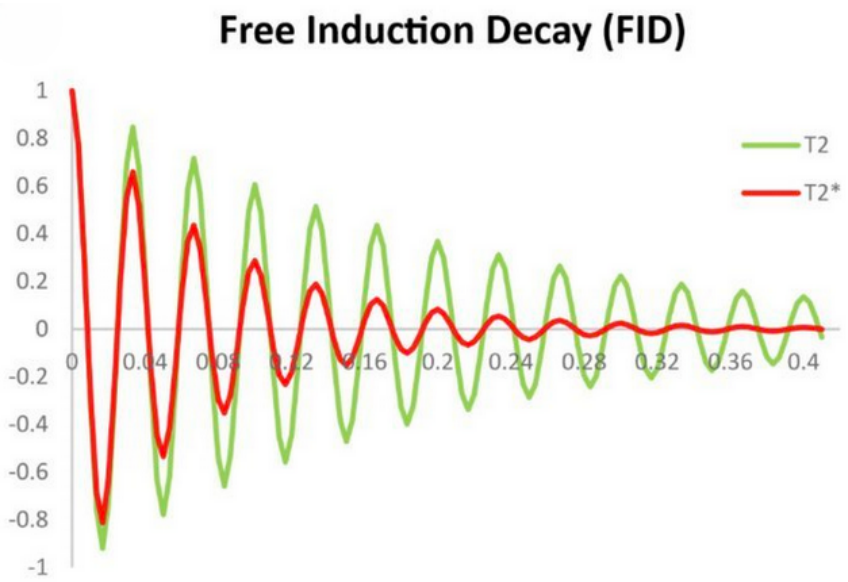

Figure 1.6: The observable NMR signal generated by non-equilibrium nuclear spin magnetization precessing about B_0 [40].

At this point, with a solid grasp of the general physical quantities involved in the production of NMR signals, it is important to link these quantities with biological processes in the human brain to progress from pure anatomical imaging to functional display. Several techniques can detect changes in metabolic activity following neural activation, including contrast fMRI, BOLD fMRI, and perfusion fMRI. Contrast fMRI requires the injection of contrast agents such as iron oxide coated with sugar or starch. Although this method can provide relatively strong signals, researchers are often reluctant to use this semi-invasive method with healthy volunteers. Perfusion fMRI utilizes Arterial Spin Labeling (ASL) to magnetically label hydrogen nuclei in arterial blood and then images their distribution in the brain. The signal received from this technique is more stable and less noisy than that of BOLD fMRI, but it is also relatively weak, and the length of image acquisition time makes it impractical for many applications. Currently the most widely used fMRI method is BOLD imaging.

1.3.3 Blood Oxygen Level Dependent *(BOLD)* Signal

The BOLD signal, captured in fMRI detects changes in HbR driven by localized changes in brain blood flow and blood oxygenation, which are coupled to underlying neuronal activity by a process termed neurovascular coupling. fMRI relies upon the measurement of T2* relaxation, which is sensitive primarily to local concentrations of paramagnetic HbR in venous blood, rendering the latter a naturally occurring contrast agent. Interpretation of the fMRI BOLD signal is intrinsically linked to understanding the underlying physiological and metabolic processes in the brain that modulate blood flow.

The BOLD effect related to neural activity arises because of two distinct phenomena. The first is that when hemoglobin (Hb)-the molecule in blood that carries oxygen-lose the oxygen to become HbR, its magnetic properties change in a subtle way: HbR is paramagnetic, and alters the magnetic susceptibility of blood, whereas HbO and the surrounding tissue H_2O are diamagnetic (see Figure 1.7). The difference in susceptibility between blood vessels and the surrounding tissue creates local magnetic field distortions that decrease the net MR signal. In the brain, a typical Oxygen Extraction Fraction (OEF)-the fraction of O_2 carried by an element of blood that is removed in passing through the capillary bed-is approximately 40% and in a

3 T magnetic field this level of HbR in the veins and capillaries is sufficient to reduce the MR signal by about 10% in the baseline state, compared to what it would be if no HbR was present.

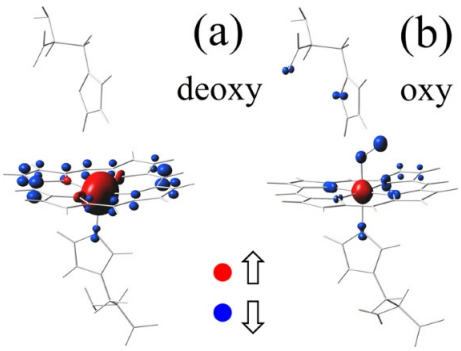

Figure 1.7: Illustation of magnetic-moment density **M(r)** for the **(a)** HbR and **(b)** HbO heme clusters at $T = 150K$. The magnitude of **M(r)** at an atomic site is proportional to the volume of the bubble at that site [41] Fig. 2 p.2).

The combination of the aforementioned with the biophysical phenomenon, that when a brain area is activated, the blood flow increases-via a process called the haemodynamic response-to a greater degree than the oxygen metabolic rate, produces a useful basis for an experimental signal aqcuisition technique. The second phenomenon leads to a reduction in the OEF, a seemingly paradoxical scenario in which the venous blood is more oxygenated, despite the increase in oxygen metabolic rate, because the blood flow has increased to a greater extent. Taken together, these two phenomena produce the BOLD effect, a local increase in the MR signal due to a reduction in the OEF during increased neural activity. [30]

A prevailing misconception is that BOLD provides a direct measurement of neuronal oxygen consumption. However, this is generally not the case; classic positive BOLD signals, seen in response to functional stimuli, represent a decrease in HbR and thus an overoxygenation of the responding region [42]. These positive BOLD responses correspond to a local, actively actuated, increase in blood flow and volume, which brings blood in sufficient excess to increase local oxygenation levels [43]. This response typically begins within about 500ms and peaks 3-5 seconds after stimulus onset Figure 1.8, even for short stimuli lasting less than 1 second, with more complex dynamics for prolonged stimuli.

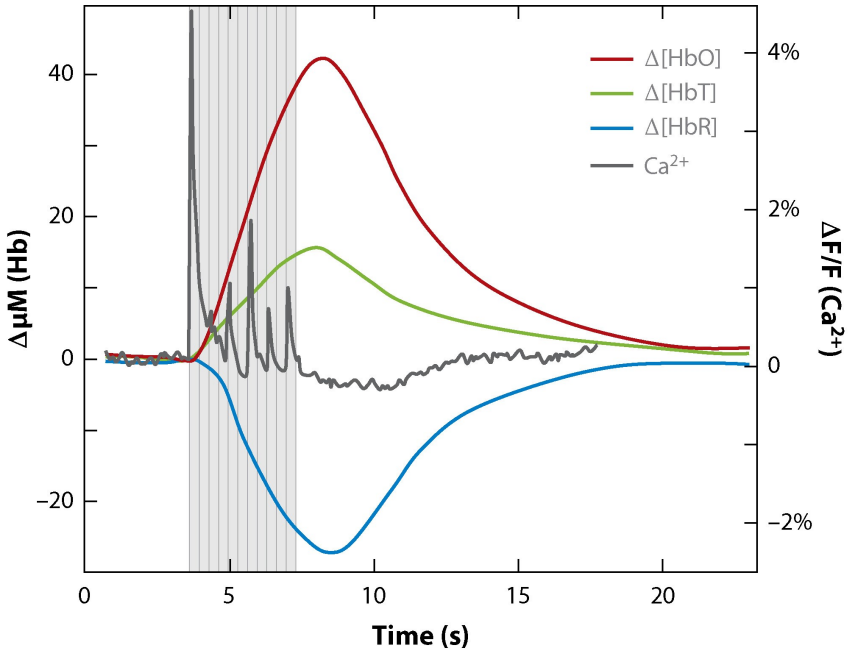

Figure 1.8: Stimulus-evoked response in somatosensory cortex of rats. Noteably, there is a distinct increase in HbT corresponding to vessel dilation and an increase in the number of red blood cells per unit volume of cortex, consistent with an increase in blood flow. HbO increases while HbR decreases, indicating a net overoxygenation of the region. The fMRI BOLD is sensitive to changes in HbR, where stimulus-evoked "positive BOLD" corresponds to the decrease in HbR shown here [44] Fig. 2 p.4).

A range of cellular mechanisms, including astrocytes, pericytes, and interneurons, have been

proposed to play a role in neurovascular coupling.[45]. For classical interpretation of BOLD signals, it is assumed that neurovascular coupling is so robust that any increase in neuronal activity generates a proportional increase in local blood flow, irrespective of brain region, brain development, and pathological state [46].

This page intentionally left blank.

Chapter 2

Data Acquisition and Manipulation

2.1 The Human Connectome Project *(HCP)*

The data handled in this project has been amassed through the HCP. The HCP was an ambitious five-year effort to characterize brain connectivity and function and their variability in healthy adults. A consortium of investigators studied a population of 1200 subjects, using multiple imaging modalities along with extensive behavioral and genetic data. The imaging modalities included diffusion imaging (dMRI), resting-state fMRI (r-fMRI), task-evoked fMRI (t-fMRI), T1-weighted (T1w) and T2-weighted (T2w) MRI for structural and myelin mapping, plus combined MEG and EEG.

During the first phase, the WU-Minn HCP consortium made a major effort to improve the methods of data acquisition and analysis, since up to that point in time, despite their great promise, all of the modalities that could be applied to *in vivo* human connectomics had serious limitations in their sensitivity, accuracy and resolution [47]. This initial phase was followed by a three-year period of data acquisition from the main cohort [48]. A key objective was to understand inter-individual variability of brain circuits, including its genetic bases and its relation to behavior, rather than merely aiming to determine the average, or typical connectivity in healthy adults. This was achieved by sampling more than three hundred young adult sibships of average size 3-4, with most of these including a monozygotic (MZ) or dizygotic (DZ) twin pair. All subjects were between 22 and 35 years old, an age range chosen to represent healthy adults beyond the age of major neurodevelopmental changes and before the onset of neurodegenerative changes. While the HCP was cross-sectional, many participants were drawn from ongoing longitudinal studies [49], [50]; they had extensive previous assessment, particularly with respect to history of the presence or absence of emotional and behavioral problems.

As for the methods, Figure 2.1 provides a high-level view of the plans used for data acquisition in Phase II of the project. Each subject spent two days at Washington University (WashU) for: behavioral assessment, whose measures spanned a broad range in the domains of cognition, emotion, perception and motor function and they were mainly drawn from the United States of America (USA) National Institute of Health (NIH) but were supplemented by a number of complementary additional measures, blood draw for eventual genotyping, and four MR scanning sessions, with three lasting one hour. The scans at WashU were carried out using a customized 3 T connectome scanner adapted from Siemens Skyra, designed to improve the quality and resolution of connectivity data; a subset of 200 subjects was also scanned at University of Minnesota (UMinn) using a new 7 T system which offers advantages, especially for the resting and task-based fMRI studies, but also for diffusion-based techniques if sufficiently short echo times can be achieved for diffusion weighting. Both systems capitalized on major improvement in advanced MR pulse sequences to obtain dMRI, r-fMRI, and t-fMRI, plus T1w and T2w anatomical scans. The t-fMRI scans incluced a range of tasks aimed at providing broad coverage of the brain and identifying as many functionally distinct domains and cortical parcels as possible. A subset of 100 subjects was also studied with combined MEG and EEG at Saint Louis University (SLU), which offer much better temporal resolutions (ms instead of s)

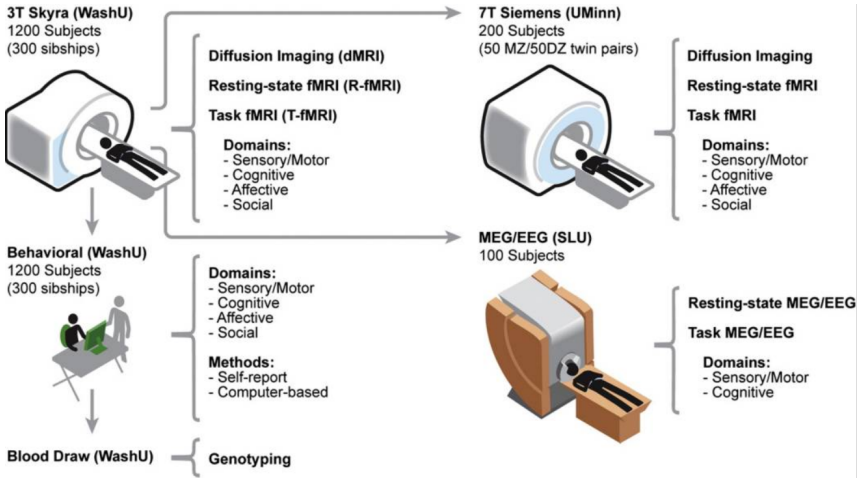

Figure 2.1: Schematic summuary for acquiring imaging, behavioral, and genetic data using MR and MEG/EEG scanners at three HCP sites.

but lower spatial resolution than MR.

2.1.1 Task-fMRI Battery of the HCP

The HCP used t-fMRI to help delineate the relationships between individual differences in the neurobiological substrates of mental processing and both functional and structural connectivity [51]. We know that there are important individual differences in suh patterns of connectivity even among persons with no diagnosable neurological or psychiatric disorders, and there is increasing evidence that this variablity is associated with alterations in cognitive and behavioral variables that constrain real world function [52]–[54]. For example, higher intelligence quotient (IQ) among healthy adults is associated with shorter path length and higher global efficiency in measures of brain functional connectivity [55] as well as greater global connectivity in prefrontal cortex [56], thus providing evidence that more efficient connectivity contributes to more effective congitive function. As another example, developmental research is increasingly suggesting that maturation of functional and structural networks in the human brain underlies key aspects of cognitive and emotional development [57]–[63].

The goal for the HCP was to identify and utilize a reliable and well-validated battery of measures that assess a wide range of human functions and behaviors in a reasonable amount of time (3-4h), to satisfy subject burden considerations. The base for the HCP's assessment was the set tools and methods developed by the NIH Toolbox of Assessment of Neurological and Behavioral function [64], including tasks developed and validated using item response theory and computer adaptive testing where appropriate and feasible. The battery was additionally expanded with tests to include measures of the following domains not covered by the Toolbox: 1) subthreshold symptoms of mood, anxiety and substance abuse; 2) additional measures of visual, memory and emotion processing; 3) personality; 4) delay discounting, as a measure of self-regulation and neuroeconomic decision making [65], [66]; 5) fluid intelligence as a measure of higher-order relational reasoning that has been linked to important individual differences in both life function and brain function [67]; 6) menstrual cycle and hormonal function for women; and 7) sleep funciton, which may be highly relevant to understanding individual differences in behavior.

The choice of t-fMRI tasks was driven by the following considerations. The aim was to identify nodes: 1) in well-characterized neural systems; 2) in as wide a range of neural systems as possible; 3) with activation locations that are reliable over time in individual subjects; 4) with activations consistently detectable in most individuals (sensitivity); and 5) that are asscosiated with a broad range of cognitive and affective processes of interest to the NIH Blueprint Institutes. In addition, it was necessary that a subset of the tasks must be suitable for task-evoked MEG (T-MEG).

Initial piloting targeted a broad range of domains that sampled diverse neural systems of interest to a wide range of individuals in the field, including: 1) visual and somatosensory-motor systems; 2) category-specific representations; 3) language function (semantic and phonological processing); 4) attention systems; 5) working memory/cognitive control systems; 6) emotion processing; 7) decision-making/reward processing; and 8) episodic memory systems.

2.1.2 Working Memory Task of the HCP

The data which is presently being examined was drawn from the WM-task which was combined with category-specific representation tasks into the following, single task paradigm [68]. One can ignore stimulus type and focus on only memory load comparisons to identify dorsal-frontal and parietal regions involved in working memory and cognitive control. Alternatively, one can collapse across memory load and focus only on stimulus type comparisons to identify temporal, occipital and parietal regions that respond to specific stimulus types.

Stimuli were projected onto a computer screen behind the subject's head within the imaging chamber. The screen was viewed by a mirror positioned approximately 8 cm above the subject's face. Participants were presented with blocks of trials that consisted of pictures of places, tools, faces and body parts (non-mutilated parts of bodies with no "nudity"). Within each run, the four different stimulus types were presented in seperate blocks. Also, within each run, half of the blocks use a 2-Back WM-task and half use a 0-Back WM-task (as a working memory comparison). In short, in "N-Back" tasks participants are presented a sequence of stimuli one-by-one. For each stimulus, they need to decide if the stimulus currently being displayed, belongs to the same category as the one presented N trials before. The factors that influence performance are not only the number N, but also the speed of presentation and the size of the set of stimuli. A 2.5 s cue indicated the task type (and target for 0-Back) at the start of the block. Each of the two runs contained eight task blocks (10 trials of 2.5 s each, for 25 s) and four fixation blocks (15 s). On each trial, the stimulus is presented for 2 s, followed by a 500 ms inter-task interval (ITI). The procedure is showcased in time order in Figure 2.2.

Segment Type	Duration (s)	N-Back Paradigm	Target Category
Setup	10	-	-
Cue	2.5	-	-
Task	25	2-Back	Body
Cue	2.5	-	-
Task	25	0-Back	Face
Fixation	15	-	-
Cue	2.5	-	-
Task	25	2-Back	Tools
Cue	2.5	-	-
Task	25	0-Back	Body
Fixation	15	-	-
Cue	2.5	-	-
Task	25	0-Back	Place
Cue	2.5	-	-
Task	25	2-Back	Face
Fixation	15	-	-
Cue	2.5	-	-
Task	25	0-Back	Tools
Cue	2.5	-	-
Task	25	2-Back	Place
Fixation	15	-	-

Figure 2.2: Display of the exact sequece of events during the WM-task paradigm.

The following event-related contrasts can potentially be gererated between 2-Back and 0-Back tasks: 1) targets for the first are 2-Back repeats while for the second, they are targets that match the cue stimulus; 2) non-targets are novel items for the former and targets that do not match the cue stimulus for the latter; and 3) lures are 1-Back and 3-Back repeats for the 2-Back tasks and repeated stimuli that do not match the cue stimulus, for 0-Back tasks.

The task design outlined above is expected to reveal distinct patterns of behavior, performance, and consequently brain activation among subjects. While there will be considerable overlap in these patterns, analysis can isolate the unique aspects, resulting in consistent and distinguishable fMRI signal from specific brain areas in response to category-specific stimuli. This pattern recognition and screening from the selection of patterns that stood out, could enable the classification of certain brain regions as more responsive and associated with processing specific types of information.

2.2 Analysis of fMRI Signal

In the analysis of fMRI signals, the primary output is a samples-by-features data matrix, similar in structure to conventional table matrices with rows and columns. Each feature represents a voxel in the brain image, and their maximum number depends on the protocol used during the fMRI scan, determined by the institution that collected the data, not by the data users. Samples are created based on the researcher's design of the analysis. Each vector of data over multiple voxels for a single sample is called a pattern, and each cell contains information that integrates the BOLD signal data as well as the researcher's analysis parameters.

The BOLD signal captured by the fMRI machine undergoes a series of processing steps unique to each analysis, resulting in varied outcomes. These outcomes are shaped by the researcher's choices, which are tailored to address the specific goals and inquiries of the research. These processing steps, which will **((give a link to the section once written))** be detailed in a later section of this paper, replace the BOLD in each cell of the data matrix with a statistical value that reflects both the signal's characteristics and the reasearcher's decisions.

At first glance, a samples-by-features matrix might seem to represent a two-dimensional analysis, but it is far more intricate. Each cell may contain data points that incorporate a single or multiple explanatory variables (EVs) meaninng each data point can be a function of several variables instead of it rather than a constant for each voxel. Additionally, sample attributes can further increase the number of variables included. These attributes, which function as headers of either rows, columns or the entire table include crucial information such as the target stimulus that produced the corresponding pattern, and the chunk to which the pattern belongs. Patterns from different chunks are considered independent of each other. Researchers may designate sample attributes differently based on logical assumptions, which can yield different practical conclusions and potentially increase the degrees of freedom in the analysis. Such a practice is shown in detail in **((link to 1vs4vs8 chunks))**.

Apart from technical decisions in data processing, the two main levers that can be manipulated are: 1) determining how many of the total EVs provided by the experiment design to include in the analysis and whether some variables can be grouped together based on the desired effect; and 2) establishing the correlation between these EVs.

2.2.1 Univariate Pattern Analysis

Uni-Variate Pattern Analysis (UPA) is a statistical approach used in neuroimaging to analyze brain activity data, particularly focusing on individual voxels. This method examines each voxel independently, assessing how its activity varies in response to different experimental conditions. Essentially, UPA measures the magnitude of an individual explanatory variable (EV) in each voxel.

For example, consider analyzing brain activity during all 0-Back trials featuring a face as a stimulus, with the only EV being the stimulus category. This analysis might show activation in both the optic nerve and the FFA during these trials. However, it cannot conclusively determine that these areas are more responsive to this stimulus category. By averaging the signal for this case and for three other identical UPAs with different stimulus categories, one might conclude that the optic nerve, showing similar activation across all categories, is not involved in category-specific information processing but is generally activated when the subject observes anything. Nevertheless, this claim would be weak, as UPA cannot distinguish what percentage of the signal magnitude is directly due to the stimulus category versus other factors.

UPA is straightforward and widely used due to its simplicity and ease of interpretation. It is particularly useful when incorporating a time element into the assessment, as the calculations for a more complex analysis over time can become excessive. However, UPA does not account for interactions between voxels, which can limit its ability to detect complex brain activity patterns and can lead to false or weak classification of brain activity patterns. Despite this limitation, UPA remains a valuable tool for identifying localized brain responses and establishing a baseline for more complex analyses.

2.2.2 Multivariate Pattern Analysis *(MVPA)*

A more appropriate tool for complex analyses and concrete conslusion would be MVPA.

2.2.3 maybe all the processing steps theoretically explained

This page intentionally left blank.

Chapter 3

Methods

3.1 My Analyses goals and my Pipeline Overview

Explain that the starting point is not 0 but it is the output of the HCP pipeline, and describe it. These sections will include snippets of software or software architecture explanation.

3.2 Pre-Processing

3.3 Statistical Analysis

3.4 Dataset Extraction - Construciton

3.5 Mask Creation - Application

3.6 Partitioning of Masked Dataset

3.7 Classifier Training and Testing

This page intentionally left blank.

Chapter 4

Classification Results

Add results text here.

This page intentionally left blank.

Chapter 5

Discussion & Conclusions

Add conclusion text here.

This page intentionally left blank.

Glossary

blob cells V1 cells that resemble kLGN neurons. They are monocular, color sensitive, characterized by small, concentric receptive fields and are found in clusters, hence the name.

connectomics The production and study of connectomes: comprehensive maps of connections within an organism's nervous system.

flip angle The amount or rotation that net magnetization experiences during application of a RF pulse.

gyromagnetic ratio The gyromagnetic ratio, a constant specific to each different nucleus.

interblob cells V1 cells, the majority of which are binocular, not color sensitive, characterized by elongated receptive fields, exhibit ocular dominance and orientation specificity, while they are found around the clusters of V1 blob cells.

Time of Echo The time between the delivery of the RF pulse and the receipt of the echo signal.

TR The amount of time that passes between consecutive acquired brain volumes.

V1 Visual area V1, the striate cortex or primary visual cortex.

V2 Visual area V2, or secondary visual cortex, also called prestriate cortex.

V3 Visual area V3, which communicates directly with the respective dorsal and ventral subsystems of V2. It is less well-defined compared to other areas of the visual cortex.

V4 Visual area V4, a midtier cortical area in the ventral visual pathway.

This page intentionally left blank.

Acronyms

ASL Arterial Spin Labeling

BOLD Blood-Oxygen-Level-Dependent

CBF Cerebral Blood Flow

CSF Cerebrospinal Fluid

dMRI diffusion imaging

DZ dizygotic

EBA Extrastriate Body Area

EEG Electroenchephalography

EV explanatory variable

EVs explanatory variables

FBA Fusiform Body Area

FFA Fusiform Face Area

FG Fusiform Gyrus

fMRI Functional Magnetic Resonance Imaging

fSTS Superior Temporal Sulcus

Hb hemoglobin

HbO Oxyhemoglobin

HbR deoxyhemoglobin

HbT total hemoglobin

HCP Human Connectome Project

IOG Inferior Occipital Gyrus

IQ intelligence quotient

IT Inferior Temporal cortex

ITI inter-task interval

LGB Lateral Geniculate Body

LOC Lateral Occipital Cortex

LOS Lateral Occipital Sulcus

MEG Magnetoenchephalogram

MOG Middle Occipital Gyrus

MR Magnetic Resonance

MRI Magnetic Resonance Imaging

MT Middle Temporal visual area

MVPA Multi-Variate Pattern Analysis

MZ monozygotic

NIH National Institute of Health

NIRS Near Infrared Spectroscopy

NMR Nuclear Magnetic Resonance

OEF Oxygen Extraction Fraction

OFA Occipital Face Area

PET Positron Emission Tomography

PPA Parahippocampal Place Area

r-fMRI resting-state fMRI

RF radio frequency

ROIs Regions of Interest

SLU Saint Louis University

t-fMRI task-evoked fMRI

T-MEG task-evoked MEG

T1w T1-weighted

T2w T2-weighted

UMinn University of Minnesota

UPA Uni-Variate Pattern Analysis

USA United States of America

WashU Washington University

WM Working Memory

Bibliography

[1] M. Gupta, A. C. Ireland, and B. Bordoni, *Neuroanatomy, Visual Pathway*. StatPearls Publishing, Dec. 2022.

[2] M. Mishkin, L. G. Ungerleider, and K. A. Macko, "Object vision and spatial vision: Two cortical pathways," *Trends in Neurosciences*, vol. 6, pp. 414–417, C Jan. 1983, ISSN: 0166-2236. DOI: 10.1016/0166-2236(83)90190-X.

[3] J. V. Haxby, C. L. Grady, B. Horwitz, *et al.*, "Dissociation of object and spatial visual processing pathways in human extrastriate cortex.," *Proceedings of the National Academy of Sciences*, vol. 88, pp. 1621–1625, 5 Mar. 1991, ISSN: 00278424. DOI: 10.1073/PNAS.88.5.1621. [Online]. Available: https://www.pnas.org/doi/abs/10.1073/pnas.88.5.1621.

[4] J. Sergent, S. Ohta, and B. Macdonald, "Functional neuroanatomy of face and object processing: A positron emission tomography study," *Brain*, vol. 115, pp. 15–36, 1 Feb. 1992, ISSN: 0006-8950. DOI: 10.1093/BRAIN/115.1.15. [Online]. Available: https://dx.doi.org/10.1093/brain/115.1.15.

[5] A. Puce, T. Allison, M. Asgari, J. C. Gore, and G. McCarthy, "Differential sensitivity of human visual cortex to faces, letterstrings, and textures: A functional magnetic resonance imaging study," *The Journal of Neuroscience*, vol. 16, p. 5205, 16 Aug. 1996, ISSN: 02706474. DOI: 10.1523/JNEUROSCI.16-16-05205.1996. [Online]. Available: /pmc/articles/PMC6579313/%20/pmc/articles/PMC6579313/?report=abstract%20https://www.ncbi.nlm.nih.gov/pmc/articles/PMC6579313/.

[6] G. Mccarthy, M. Luby, J. Gore, and P. Goldman-Rakic, "Infrequent events transiently activate human prefrontal and parietal cortex as measured by functional mri," *Journal of neurophysiology*, vol. 77, pp. 1630–1634, 3 1997, ISSN: 0022-3077. DOI: 10.1152/JN.1997.77.3.1630. [Online]. Available: https://pubmed.ncbi.nlm.nih.gov/9084626/.

[7] N. Kanwisher, J. McDermott, and M. M. Chun, "The fusiform face area: A module in human extrastriate cortex specialized for face perception," *The Journal of Neuroscience*, vol. 17, p. 4302, 11 Jun. 1997, ISSN: 02706474. DOI: 10.1523/JNEUROSCI.17-11-04302.1997. [Online]. Available: /pmc/articles/PMC6573547/%20/pmc/articles/PMC6573547/?report=abstract%20https://www.ncbi.nlm.nih.gov/pmc/articles/PMC6573547/.

[8] N. Kanwisher and G. Yovel, "The fusiform face area: A cortical region specialized for the perception of faces," *Philosophical Transactions of the Royal Society B: Biological Sciences*, vol. 361, p. 2109, 1476 Dec. 2006, ISSN: 09628436. DOI: 10.1098/RSTB.2006.1934. [Online]. Available: /pmc/articles/PMC1857737/%20/pmc/articles/PMC1857737/?report=abstract%20https://www.ncbi.nlm.nih.gov/pmc/articles/PMC1857737/.

[9] R. Epstein and N. Kanwisher, "A cortical representation of the local visual environment," *Nature 1998 392:6676*, vol. 392, pp. 598–601, 6676 Apr. 1998, ISSN: 1476-4687. DOI: 10.1038/33402. [Online]. Available: https://www.nature.com/articles/33402.

[10] R. Epstein, A. Harris, D. Stanley, and N. Kanwisher, "The parahippocampal place area: Recognition, navigation, or encoding?" *Neuron*, vol. 23, pp. 115–125, 1 May 1999, ISSN: 0896-6273. DOI: 10.1016/S0896-6273(00)80758-8.

[11] R. Epstein, K. S. Graham, and P. E. Downing, "Viewpoint-specific scene representations in human parahippocampal cortex," *Neuron*, vol. 37, pp. 865–876, 5 Mar. 2003, ISSN: 08966273. DOI: 10.1016/S0896-6273(03)00117-X. [Online]. Available: https://pubmed.ncbi.nlm.nih.gov/12628176/.

[12] S. Park and M. M. Chun, "Different roles of the parahippocampal place area (ppa) and retrosplenial cortex (rsc) in panoramic scene perception," *NeuroImage*, vol. 47, p. 1747, 4 Oct. 2009, ISSN: 10538119. DOI: 10.1016/J.NEUROIMAGE.2009.04.058. [Online]. Available: /pmc/articles/PMC2753672/%20/pmc/articles/PMC2753672/?report=abstract%20https://www.ncbi.nlm.nih.gov/pmc/articles/PMC2753672/.

[13] R. Malach, J. B. Reppas, R. R. Benson, *et al.*, "Object-related activity revealed by functional magnetic resonance imaging in human occipital cortex.," *Proceedings of the National Academy of Sciences*, vol. 92, pp. 8135–8139, 18 Aug. 1995, ISSN: 00278424. DOI: 10.1073/PNAS.92.18.8135. [Online]. Available: https://www.pnas.org/doi/abs/10.1073/pnas.92.18.8135.

[14] N. Kanwisher, M. M. Chun, J. McDermott, and P. J. Ledden, "Functional imaging of human visual recognition," *Cognitive Brain Research*, vol. 5, pp. 55–67, 1-2 Dec. 1996, ISSN: 0926-6410. DOI: 10.1016/S0926-6410(96)00041-9.

[15] K. Grill-Spector, T. Kushnir, T. Hendler, S. Edelman, Y. Itzchak, and R. Malach, "A sequence of object-processing stages revealed by fmri in the human occipital lobe," *Human Brain Mapping*, vol. 6, no. 4, pp. 316–328, 1998, ISSN: 1065-9471. DOI: 10.1002/(sici)1097-0193(1998)6:4<316::aid-hbm9>3.0.co;2-6. [Online]. Available: http://dx.doi.org/10.1002/(SICI)1097-0193(1998)6:4%3C316::AID-HBM9%3E3.0.CO;2-6.

[16] S. Murtha, H. Chertkow, M. Beauregard, and A. Evans, "The neural substrate of picture naming," *Journal of Cognitive Neuroscience*, vol. 11, pp. 399–423, 4 Jul. 1999, ISSN: 0898-929X. DOI: 10.1162/089892999563508. [Online]. Available: https://dx.doi.org/10.1162/089892999563508.

[17] K. Grill-Spector, Z. Kourtzi, and N. Kanwisher, "The lateral occipital complex and its role in object recognition," *Vision Research*, vol. 41, pp. 1409–1422, 10-11 May 2001, ISSN: 0042-6989. DOI: 10.1016/S0042-6989(01)00073-6.

[18] P. E. Downing, Y. Jiang, M. Shuman, and N. Kanwisher, "A cortical area selective for visual processing of the human body," *Science*, vol. 293, pp. 2470–2473, 5539 Sep. 2001, ISSN: 00368075. DOI: 10.1126/SCIENCE.1063414. [Online]. Available: https://www.science.org/doi/10.1126/science.1063414.

[19] M. V. Peelen and P. E. Downing, "Selectivity for the human body in the fusiform gyrus," *Journal of Neurophysiology*, vol. 93, pp. 603–608, 1 Jan. 2005, ISSN: 00223077. DOI: 10.1152/JN.00513.2004/ASSET/IMAGES/LARGE/Z9K0010543090003.JPEG. [Online]. Available: https://journals.physiology.org/doi/10.1152/jn.00513.2004.

[20] M. Spiridon, B. Fischl, and N. Kanwisher, "Location and spatial profile of category-specific regions in human extrastriate cortex," *Human Brain Mapping*, vol. 27, pp. 77–89, 1 Jan. 2006, ISSN: 10659471. DOI: 10.1002/HBM.20169.

[21] K. S. Weiner and K. Grill-Spector, "Sparsely-distributed organization of face and limb activations in human ventral temporal cortex," *NeuroImage*, vol. 52, pp. 1559–1573, 4 Oct. 2010, ISSN: 1053-8119. DOI: 10.1016/J.NEUROIMAGE.2010.04.262.

[22] L. Amoruso, B. Couto, and A. Ibáñez, "Beyond extrastriate body area (eba) and fusiform body area (fba): Context integration in the meaning of actions," *Frontiers in Human Neuroscience*, vol. 5, p. 13143, Nov. 2011, ISSN: 16625161. DOI: 10.3389/FNHUM.2011.00124/BIBTEX.

[23] A. Pann, M. Bonnard, O. Felician, and P. Romaiguère, "The extrastriate body area and identity processing: An fmri guided tms study," *Physiological Reports*, vol. 9, 8 Apr. 2021, ISSN: 2051817X. DOI: 10.14814/PHY2.14711. [Online]. Available: /pmc/articles/PMC8090840/%20/pmc/articles/PMC8090840/?report=abstract%20https://www.ncbi.nlm.nih.gov/pmc/articles/PMC8090840/.

[24] J. C. Taylor, A. J. Wiggett, and P. E. Downing, "Functional mri analysis of body and body part representations in the extrastriate and fusiform body areas," *Journal of Neurophysiology*, vol. 98, pp. 1626–1633, 3 Sep. 2007, ISSN: 00223077. DOI: 10.1152/JN.00012.2007/ASSET/IMAGES/LARGE/Z9K0090783830004.JPEG. [Online]. Available: https://journals.physiology.org/doi/10.1152/jn.00012.2007.

[25] *The visual centers of the brain | the visionhelp blog*. [Online]. Available: https://visionhelp.wordpress.com/2018/07/04/the-visual-centers-of-the-brain/.

[26] *Prosopagnosia | fusiform face area functions and impact*. [Online]. Available: https://prosopagnosiabytmayo.wordpress.com/.

[27] R. F. Schwarzlose, C. I. Baker, and N. Kanwisher, "Separate face and body selectivity on the fusiform gyrus," *The Journal of neuroscience : the official journal of the Society for Neuroscience*, vol. 25, pp. 11 055–11 059, 47 Nov. 2005, ISSN: 1529-2401. DOI: 10.1523/JNEUROSCI.2621-05.2005. [Online]. Available: https://pubmed.ncbi.nlm.nih.gov/16306418/.

[28] M. Li, H. Huang, B. Guo, and M. Meng, "Distinct response properties between the ffa to faces and the ppa to houses," *Brain and Behavior*, vol. 12, e2706, 8 Aug. 2022, ISSN: 2162-3279. DOI: 10.1002/BRB3.2706. [Online]. Available: https://onlinelibrary.wiley.com/doi/full/10.1002/brb3.2706%20https://onlinelibrary.wiley.com/doi/abs/10.1002/brb3.2706%20https://onlinelibrary.wiley.com/doi/10.1002/brb3.2706.

[29] G. XUE, C. CHEN, Z.-L. LU, and Q. DONG, "Brain imaging techniques and their applications in decision-making research," *Xin li xue bao. Acta psychologica Sinica*, vol. 42, p. 120, 1 Feb. 2010, ISSN: 0439-755X. DOI: 10.3724/SP.J.1041.2010.00120. [Online]. Available: /pmc/articles/PMC2849100/%20/pmc/articles/PMC2849100/?report=abstract%20https://www.ncbi.nlm.nih.gov/pmc/articles/PMC2849100/.

[30] R. B. Buxton, "The physics of functional magnetic resonance imaging (fmri)," *Reports on Progress in Physics*, vol. 76, 9 Sep. 2013, ISSN: 00344885. DOI: 10.1088/0034-4885/76/9/096601.

[31] A. Suriaga, R. M. Tappen, E. R. Aston, L. Chiang-Hanisko, and D. Newman, "The physics of fmri," *Journal of Nursing Scholarship*, vol. 26, pp. 623–636, 3 May 2009, ISSN: 15475069. [Online]. Available: https://www.psychiatrictimes.com/view/physics-fmri.

[32] *T1 relaxation - questions and answers in mri*. [Online]. Available: https://mriquestions.com/what-is-t1.html.

[33] J. A. Detre, J. S. Leigh, D. S. Williams, and A. P. Koretsky, "Perfusion imaging," *Magnetic Resonance in Medicine*, vol. 23, pp. 37–45, 1 Jan. 1992, ISSN: 1522-2594. DOI: 10.1002/MRM.1910230106. [Online]. Available: https://onlinelibrary.wiley.com/doi/full/10.1002/mrm.1910230106%20https://onlinelibrary.wiley.com/doi/abs/10.1002/mrm.1910230106%20https://onlinelibrary.wiley.com/doi/10.1002/mrm.1910230106.

[34] *T2 (spin-spin) relaxation - questions and answers in mri*. [Online]. Available: https://mriquestions.com/what-is-t2.html.

[35] *T2* vs t2 relaxation time - questions and answers in mri*. [Online]. Available: https://www.mriquestions.com/t2-vs-t2.html.

[36] S. G. Kim and S. Ogawa, "Biophysical and physiological origins of blood oxygenation level-dependent fmri signals," *Journal of Cerebral Blood Flow and Metabolism*, vol. 32, pp. 1188–1206, 7 Jul. 2012, ISSN: 0271678X. DOI: 10.1038/JCBFM.2012.23/ASSET/IMAGES/LARGE/10.1038_JCBFM.2012.23-FIG6.JPEG. [Online]. Available: https://journals.sagepub.com/doi/full/10.1038/jcbfm.2012.23.

[37] H. Ito, I. Kanno, H. Iida, *et al.*, "Arterial fraction of cerebral blood volume in humans measured by positron emission tomography," *Annals of Nuclear Medicine*, vol. 15, pp. 111–116, 2 2001, ISSN: 09147187. DOI: 10.1007/BF02988600/METRICS. [Online]. Available: https://link.springer.com/article/10.1007/BF02988600.

[38] H. An and W. Lin, "Cerebral venous and arterial blood volumes can be estimated separately in humans using magnetic resonance imaging," *Magnetic Resonance in Medicine*, vol. 48, pp. 583–588, 4 Oct. 2002, ISSN: 1522-2594. DOI: 10.1002/MRM.10257. [Online]. Available: https://onlinelibrary.wiley.com/doi/full/10.1002/mrm.10257%20https://onlinelibrary.wiley.com/doi/abs/10.1002/mrm.10257%20https://onlinelibrary.wiley.com/doi/10.1002/mrm.10257.

[39] H. An and W. Lin, "Cerebral oxygen extraction fraction and cerebral venous blood volume measurements using mri: Effects of magnetic field variation," *Magnetic Resonance in Medicine*, vol. 47, pp. 958–966, 5 May 2002, ISSN: 1522-2594. DOI: 10.1002/MRM.10148. [Online]. Available: https://onlinelibrary.wiley.com/doi/full/10.1002/mrm.10148%20https://onlinelibrary.wiley.com/doi/abs/10.1002/mrm.10148%20https://onlinelibrary.wiley.com/doi/10.1002/mrm.10148.

[40] *Part 2 – t2 relaxation: Definition, measurement and practical implications! — nanalysis*. [Online]. Available: https://www.nanalysis.com/nmready-blog/2020/6/1/part-2-t2-relaxation-definition-measurement-and-practical-implications-wps35.

[41] S. Mayda, Z. Kandemir, N. Bulut, and S. Maekawa, "Magnetic mechanism for the biological functioning of hemoglobin," *Scientific Reports*, vol. 10, 1 Dec. 2020, ISSN: 20452322. DOI: 10.1038/s41598-020-64364-y. [Online]. Available: https://www.nature.com/articles/s41598-020-64364-y.

[42] D. Attwell and C. Iadecola, "The neural basis of functional brain imaging signals," *Trends in neurosciences*, vol. 25, no. 12, pp. 621–625, 2002.

[43] M. E. Raichle, *Neuroimaging of human brain function*, 1998. [Online]. Available: www.pnas.org..

[44] E. M. C. Hillman, "Optical brain imaging in vivo: Techniques and applications from animal to man," *Journal of Biomedical Optics*, vol. 12, p. 051 402, 5 2007, ISSN: 10833668. DOI: 10.1117/1.2789693.

[45] E. M. Hillman, *Coupling mechanism and significance of the bold signal: A status report*, 2014. DOI: 10.1146/annurev-neuro-071013-014111.

[46] N. K. Logothetis, "Neurovascular uncoupling: Much ado about nothing," *Frontiers in Neuroenergetics*, vol. 2, 2010. DOI: 10.3389/fnene.2010.00002.

[47] D. C. V. Essen and K. Ugurbil, "The future of the human connectome," *NeuroImage*, vol. 62, pp. 1299–1310, 2 Aug. 2012, ISSN: 1053-8119. DOI: 10.1016/J.NEUROIMAGE.2012.01.032.

[48] D. C. V. Essen, K. Ugurbil, E. Auerbach, *et al.*, "The human connectome project: A data acquisition perspective," *NeuroImage*, vol. 62, p. 2222, 4 Oct. 2012, ISSN: 10538119. DOI: 10.1016/J.NEUROIMAGE.2012.02.018. [Online]. Available: /pmc/articles/PMC3606888/%20/pmc/articles/PMC3606888/?report=abstract%20https://www.ncbi.nlm.nih.gov/pmc/articles/PMC3606888/.

[49] C. E. Sartor, K. K. Bucholz, E. C. Nelson, P. A. Madden, M. T. Lynskey, and A. C. Heath, "Reporting bias in the association between age at first alcohol use and heavy episodic drinking," *Alcoholism: Clinical and Experimental Research*, vol. 35, pp. 1418–1425, 8 Aug. 2011, ISSN: 1530-0277. DOI: 10.1111/J.1530-0277.2011.01477.X. [Online]. Available: https://onlinelibrary.wiley.com/doi/full/10.1111/j.1530-0277.2011.01477.x%20https://onlinelibrary.wiley.com/doi/abs/10.1111/j.1530-0277.2011.01477.x%20https://onlinelibrary.wiley.com/doi/10.1111/j.1530-0277.2011.01477.x.

[50] E. L. Edens, A. L. Glowinski, M. L. Pergadia, C. N. Lessov-Schlaggar, and K. K. Bucholz, "Nicotine addiction in light smoking african american mothers," *Journal of Addiction Medicine*, vol. 4, pp. 55–60, 1 Mar. 2010, ISSN: 19320620. DOI: 10.1097/ADM.0B013E3181AF111E. [Online]. Available: https://journals.lww.com/journaladdictionmedicine/fulltext/2010/03000/nicotine_addiction_in_light_smoking_african.8.aspx.

[51] D. M. Barch, G. C. Burgess, M. P. Harms, *et al.*, "Function in the human connectome: Task-fmri and individual differences in behavior," *NeuroImage*, vol. 80, pp. 169–189, Oct. 2013, ISSN: 1053-8119. DOI: 10.1016/J.NEUROIMAGE.2013.05.033.

[52] D. S. Bassett, E. T. Bullmore, A. Meyer-Lindenberg, J. A. Apud, D. R. Weinberger, and R. Coppola, "Cognitive fitness of cost-efficient brain functional networks," *Proceedings of the National Academy of Sciences of the United States of America*, vol. 106, pp. 11 747–11 752, 28 Jul. 2009, ISSN: 1091-6490. DOI: 10.1073/PNAS.0903641106. [Online]. Available: https://pubmed.ncbi.nlm.nih.gov/19564605/.

[53] M. Song, Y. Zhou, J. Li, *et al.*, "Brain spontaneous functional connectivity and intelligence," *NeuroImage*, vol. 41, pp. 1168–1176, 3 Jul. 2008, ISSN: 1053-8119. DOI: 10.1016/J.NEUROIMAGE.2008.02.036. [Online]. Available: https://pubmed.ncbi.nlm.nih.gov/18434203/.

[54] M. P. V. D. Heuvel, C. J. Stam, R. S. Kahn, and H. E. H. Pol, "Efficiency of functional brain networks and intellectual performance," *The Journal of neuroscience : the official journal of the Society for Neuroscience*, vol. 29, pp. 7619–7624, 23 Jun. 2009, ISSN: 1529-2401. DOI: 10.1523/JNEUROSCI.1443-09.2009. [Online]. Available: https://pubmed.ncbi.nlm.nih.gov/19515930/.

[55] Y. Li, Y. Liu, J. Li, *et al.*, "Brain anatomical network and intelligence," *PLoS computational biology*, vol. 5, 5 2009, ISSN: 1553-7358. DOI: 10.1371/JOURNAL.PCBI.1000395. [Online]. Available: https://pubmed.ncbi.nlm.nih.gov/19492086/.

[56] M. W. Cole, T. Yarkoni, G. Repovš, A. Anticevic, and T. S. Braver, "Global connectivity of prefrontal cortex predicts cognitive control and intelligence," *The Journal of neuroscience : the official journal of the Society for Neuroscience*, vol. 32, pp. 8988–8999, 26 Jun. 2012, ISSN: 1529-2401. DOI: 10.1523/JNEUROSCI.0536-12.2012. [Online]. Available: https://pubmed.ncbi.nlm.nih.gov/22745498/.

[57] D. A. Fair, N. U. Dosenbach, J. A. Church, *et al.*, "Development of distinct control networks through segregation and integration," *Proceedings of the National Academy of Sciences of the United States of America*, vol. 104, pp. 13 507–13 512, 33 Aug. 2007, ISSN: 0027-8424. DOI: 10.1073/PNAS.0705843104. [Online]. Available: https://pubmed.ncbi.nlm.nih.gov/17679691/.

[58] D. A. Fair, A. L. Cohen, J. D. Power, *et al.*, "Functional brain networks develop from a "local to distributed" organization," *PLoS computational biology*, vol. 5, 5 2009, ISSN: 1553-7358. DOI: 10.1371/JOURNAL.PCBI.1000381. [Online]. Available: https://pubmed.ncbi.nlm.nih.gov/19412534/.

[59] K. Hwang, M. N. Hallquist, and B. Luna, "The development of hub architecture in the human functional brain network," *Cerebral cortex (New York, N.Y. : 1991)*, vol. 23, pp. 2380–2393, 10 Oct. 2013, ISSN: 1460-2199. DOI: 10.1093/CERCOR/BHS227. [Online]. Available: https://pubmed.ncbi.nlm.nih.gov/22875861/.

[60] D. Imperati, S. Colcombe, C. Kelly, *et al.*, "Differential development of human brain white matter tracts," *PloS one*, vol. 6, 8 2011, ISSN: 1932-6203. DOI: 10.1371/JOURNAL.PONE.0023437. [Online]. Available: https://pubmed.ncbi.nlm.nih.gov/21909351/.

[61] M. C. Stevens, P. Skudlarski, G. D. Pearlson, and V. D. Calhoun, "Age-related cognitive gains are mediated by the effects of white matter development on brain network integration," *NeuroImage*, vol. 48, pp. 738–746, 4 Dec. 2009, ISSN: 1095-9572. DOI: 10.1016/J.NEUROIMAGE.2009.06.065. [Online]. Available: https://pubmed.ncbi.nlm.nih.gov/19577651/.

[62] K. Supekar, M. Musen, and V. Menon, "Development of large-scale functional brain networks in children," *PLoS biology*, vol. 7, 7 Jul. 2009, ISSN: 1545-7885. DOI: 10.1371/JOURNAL.PBIO.1000157. [Online]. Available: https://pubmed.ncbi.nlm.nih.gov/19621066/.

[63] X. N. Zuo, C. Kelly, A. D. Martino, *et al.*, "Growing together and growing apart: Regional and sex differences in the lifespan developmental trajectories of functional homotopy," *The Journal of neuroscience : the official journal of the Society for Neuroscience*, vol. 30, pp. 15 034–15 043, 45 Nov. 2010, ISSN: 1529-2401. DOI: 10.1523/JNEUROSCI.2612-10.2010. [Online]. Available: https://pubmed.ncbi.nlm.nih.gov/21068309/.

[64] *Home - nih toolbox*. [Online]. Available: https://nihtoolbox.org/.

[65] J. W. Dalley, A. C. Mar, D. Economidou, and T. W. Robbins, "Neurobehavioral mechanisms of impulsivity: Fronto-striatal systems and functional neurochemistry," *Pharmacology, biochemistry, and behavior*, vol. 90, pp. 250–260, 2 Aug. 2008, ISSN: 0091-3057. DOI: 10.1016/J.PBB.2007.12.021. [Online]. Available: https://pubmed.ncbi.nlm.nih.gov/18272211/.

[66] N. A. Shamosh, C. G. DeYoung, A. E. Green, *et al.*, "Individual differences in delay discounting: Relation to intelligence, working memory, and anterior prefrontal cortex," *Psychological science*, vol. 19, pp. 904–911, 9 Sep. 2008, ISSN: 1467-9280. DOI: 10.1111/J.1467-9280.2008.02175.X. [Online]. Available: https://pubmed.ncbi.nlm.nih.gov/18947356/.

[67] G. C. Burgess, J. R. Gray, A. R. Conway, and T. S. Braver, "Neural mechanisms of interference control underlie the relationship between fluid intelligence and working memory span," *Journal of experimental psychology. General*, vol. 140, pp. 674–692, 4 Nov. 2011, ISSN: 1939-2222. DOI: 10.1037/A0024695. [Online]. Available: https://pubmed.ncbi.nlm.nih.gov/21787103/.

[68] *Connectome - hcp 3t task fmri protocol overview*. [Online]. Available: https://www.humanconnectome.org/hcp-protocols-ya-task-fmri.